![Aalto University logo]

Najafi Jabdaraghi, Robab; Golubev, Dmitry; Pekola, J.P.; Peltonen, Joonas

Noise of a superconducting magnetic flux sensor based on a proximity Josephson junction

SCIENTIFIC REPORTS

Noise of a superconducting magnetic flux sensor based on a proximity Josephson junction

R. N. Jabdaraghi [ID], D. S. Golubev, J. P. Pekola & J. T. Peltonen

We demonstrate simultaneous measurements of DC transport properties and flux noise of a hybrid superconducting magnetometer based on the proximity effect (superconducting quantum interference proximity transistor, SQUIPT). The noise is probed by a cryogenic amplifier operating in the frequency range of a few MHz. In our non-optimized device, we achieve minimum flux noise ~4 $\mu\Phi_0$/Hz$^{1/2}$, set by the shot noise of the probe tunnel junction. The flux noise performance can be improved by further optimization of the SQUIPT parameters, primarily minimization of the proximity junction length and cross section. Furthermore, the experiment demonstrates that the setup can be used to investigate shot noise in other nonlinear devices with high impedance. This technique opens the opportunity to measure sensitive magnetometers including SQUIPT devices with very low dissipation.

Measuring noise provides an uncompromising test of microscopic and nanoscopic superconducting sensors[1–5], such as superconducting quantum interference devices (SQUIDs), for ultra-sensitive detection of weak and local magnetic signals. A hybrid superconducting magnetometer[6, 7] based on the proximity effect[8] (superconducting quantum interference proximity transistor, SQUIPT[9]) has demonstrated in experiments high responsivity to magnetic flux[9–12] and theoretically[13] the noise is predicted to be very low, comparable to or below 50 nΦ_0/Hz$^{1/2}$ obtained with state-of-the-art nanoSQUIDs[4, 5]. Yet the intrinsic limits to flux noise performance of such a device have not been experimentally investigated in detail up to now. Here, we present a measurement of flux noise of a SQUIPT using a cryogenic amplifier[14–17] operating in the frequency range of a few MHz.

A SQUIPT interferometer consists of a superconducting loop interrupted by a short normal-metal wire in direct metal-to-metal contact while an additional superconducting probe electrode is tunnel-coupled to the normal region, cf. Fig. 1(a). Its operation relies on the phase dependence of the density of states (DoS) in the normal part[18], probed via the tunnel junction. The figure of merit of a SQUIPT magnetometer is the noise-equivalent flux (NEF) or flux sensitivity[19], which has been considered theoretically in Ref. Giazotto2011. In the earliest experimental realization[9], the NEF was limited by the preamplifier contribution to the noise, and estimated to be ~20 $\mu\Phi_0$/Hz$^{1/2}$. In a subsequent optimized device with a shorter proximity junction, 500 nΦ_0/Hz$^{1/2}$ has been obtained at 240 mK in a low-frequency (sub-kHz) cross-correlation measurement, still limited by the room-temperature amplifier noise[12]. Recently, 260 nΦ_0/Hz$^{1/2}$ at 1 K was reported for a fully superconducting device[20]. However, the challenging task has remained to observe directly the non-bandwidth-limited intrinsic flux noise performance of the hybrid superconducting magnetometer devices, predicted to be determined by shot noise in the current through the probe tunnel junction[13].

Besides hindering sensor operation, the shot noise[21, 22] in the electrical current of a biased conductor provides information on quantum transport in mesoscopic structures beyond the average current[23]. It has been measured in various systems, including quantum point contacts (QPCs)[24, 25] and quantum dots (QDs)[26], and found to provide an accurate means of primary thermometry for metallic tunnel junctions[27, 28] and recently for QPCs as well[29]. A successful technique for measuring the shot noise of high-impedance semiconducting samples relies on a cryogenic amplifier based on a high electron mobility transistor (HEMT) and an RLC tank circuit with resonance frequency of a few MHz[14–16]. Such an approach avoids the ubiquitous amplifier 1/f noise and signal loss due to low pass filter formed by cable capacitance and the high sample inductance. For enhanced sensitivity, the method extends straightforwardly to cross-correlation of signals from two amplifiers[14], and its adaptations have been employed to study the noise of QPCs[30, 31] and QDs[32, 33], including demonstration of the quantum of thermal

Low Temperature Laboratory, Department of Applied Physics, Aalto University School of Science, P.O. Box 13500, FI-00076, Aalto, Finland. Correspondence and requests for materials should be addressed to R.N.J. (email: robab. najafi.jabdaraghi@aalto.fi)
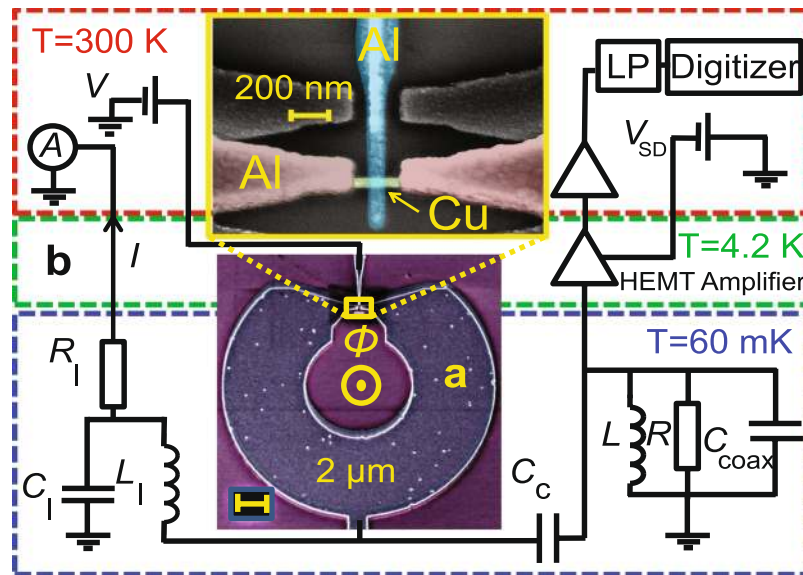
Figure 1. Typical sample and the noise measurement setup. **(a)** False color scanning electron micrograph of the SQUIPT device, together with a zoomed-in view of the Cu island (green) embedded in the superconducting Al loop (brown). The Al tunnel probe (blue) contacts the middle of the proximity SNS junction. **(b)** Schematic view of the DC and noise measurement system in the dilution refrigerator. Fluctuations of current through the sample are converted to voltage noise at the HEMT amplifier input by a resonant circuit formed mainly by the inductors L and L_l on the sample holder, and the distributed cable capacitance C_{coax} that connects the sample to the cryogenic amplifier residing directly in the helium bath.

conductance for heat flow in a single electronic channel[34]. In this work we use the technique to characterize the flux noise of a hybrid superconducting tunnel junction magnetometer. Here we present simultaneous measurements of the DC transport properties and current noise of a SQUIPT interferometer, and use them to infer a NEF $\approx 4\,\mu\Phi_0/Hz^{1/2}$ in the non-optimized structure with a proximity SNS junction of length $l \approx 245\,nm$. We show that the low-temperature readout of RLC filtered shot noise can be applied to the study of nonlinear devices once changes in the differential resistance are taken into account, cf. gate-tunable semiconducting devices where the resistance depends only weakly on the bias voltage.

Results

Noise measurement setup. A typical SQUIPT based on a superconducting aluminium loop placed into a perpendicular magnetic field is presented in Fig. 1(a), with an enlarged view of the weak link region depicted in the top inset. It is fabricated using conventional methods of electron beam lithography and metal deposition through a suspended mask (see further fabrication details in the Methods Section). The noise measurement setup is installed in a ^{3}He/^{4}He dilution refrigerator with base temperature close to 60 mK as shown in Fig. 1(b). As the main elements, our home made double-HEMT cryogenic amplifier[17] (see Fig. 6 in the Methods Section for amplifier characterization at room temperature and 4.2 K) and the inductors of the LC resonant circuit are placed in the liquid helium bath and on the sample holder at base temperature, respectively. The voltage source V_{SD} is used to bias the amplifier. A bias voltage V is applied to the SQUIPT tunnel probe electrode, and the average current I is measured with a room-temperature current amplifier through the line with inductor L_l. This line is low-pass filtered by the resistance $R_l = 330\,\Omega$ and capacitance $C_l = 22\,nF$. An identical filter is included in the biasing line of the tunnel probe but omitted in Fig. 1(b) for clarity.

Simultaneously with measurement of the average current I, current noise through the SQUIPT is probed by the HEMT amplifier via the capacitor C_c. At frequencies of the order of the resonance at $f_0 = 1/(2\pi\sqrt{L'C_{coax}}) \approx 4.2\,MHz$, formed by the inductance $L' = (L^{-1} + L_l^{-1})^{-1} \approx 16.5\,\mu H$ (due to the coils $L = L_l = 33\,\mu H$ on the sample holder) and the capacitance $C_{coax} \approx 92\,pF$ (mainly due to distributed cable capacitance between the sample holder and the amplifier), the capacitors $C_c = C_l$ can be considered as electrical shorts. Importantly, this results in a robust peak signature of the white shot noise of the sample, filtered by the characteristic band-pass response of the $RL'C_{coax}$ circuit, to be present in the observed voltage noise spectral density. In Fig. 1(b), the phenomenological resistor $R \gtrsim 50\,k\Omega$ denotes the parasitic losses in the circuit, mainly the inductors L and L_l. It accounts for the losses in the circuit when the differential resistance of the sample $R_S(V, \Phi) = dV/dI \gtrsim R$. The signal is further amplified by another stage (SRS SR445A) at room temperature, and low pass (LP) filtered by a commercial 5 MHz filter to avoid aliasing. The amplified voltage signal is finally captured by a 16-bit digitizer running continuously at 50 MSamples/s, converted into spectral density of voltage noise by windowing and Fast Fourier Transform of blocks with typically 2^{15} samples[14], and a desired number of spectra are averaged together to improve the signal-to-noise ratio.

DC transport measurements. Figure 2(a) displays the experimental current–voltage (IV) characteristics of the device recorded at $T = 60\,mK$ at two different magnetic fields, $\Phi = 0$ and $\Phi = 0.5\,\Phi_0$, which correspond to
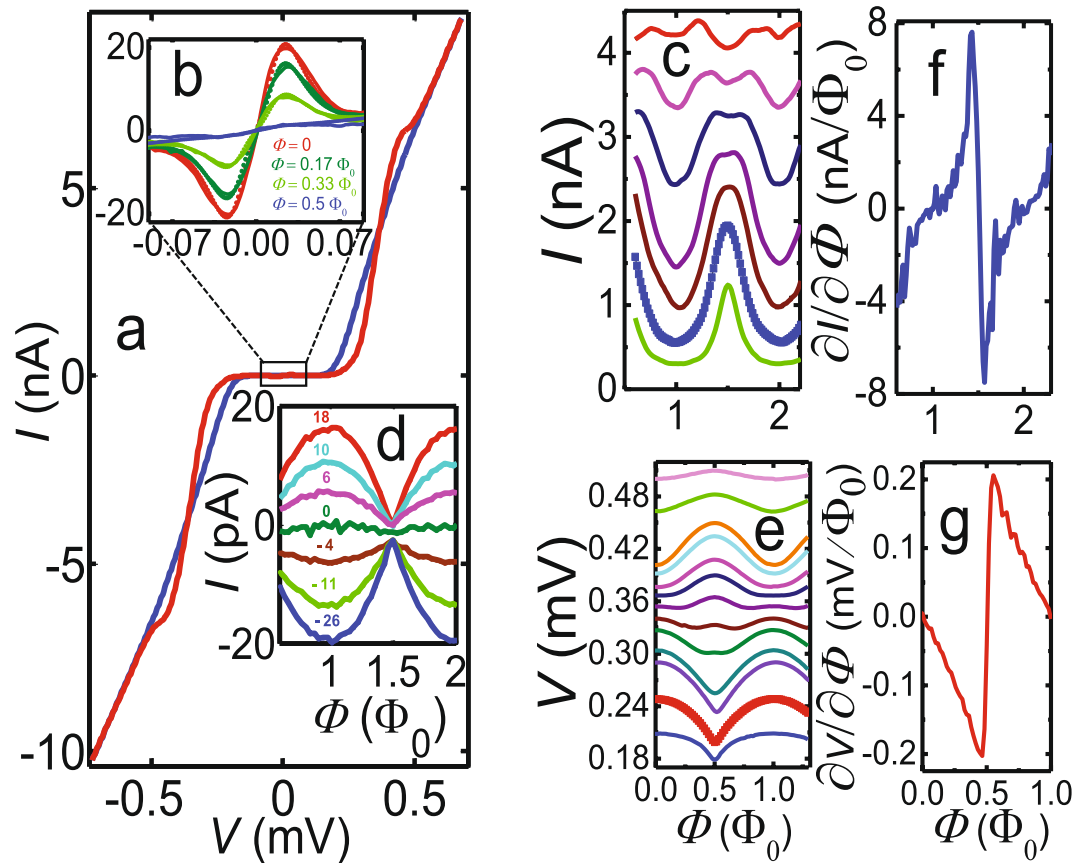
Figure 2. DC transport measurements. **(a)** IV characteristics at $T = 60$ mK, measured at two values of magnetic flux $\Phi = 0$ (red solid line) and $\Phi = 0.5\,\Phi_0$ (blue solid line), respectively. **(b)** Flux modulation of the IV curve (solid lines) around zero bias voltage at four values of magnetic flux between $\Phi = 0$ and $\Phi = 0.5\,\Phi_0$, together with the theoretical model at each flux (dotted lines). **(c)** Current modulation $I(\Phi)$ at various fixed bias voltages $V \gtrsim \Delta/e$, and **(d)**, in the sub-gap region close to zero bias voltage. Here the bias voltages are indicated in microvolts. **(e)** Measured flux-to-voltage curves $V(\Phi)$ at several values of the bias current through the device. **(f)** Current responsivity $\partial I/\partial \Phi$ and **(g)**, voltage responsivity $\partial V/\partial \Phi$ as functions of the magnetic flux at the optimum bias points, $V = 0.249$ mV and $I = 4.2$ nA, respectively.

maximum and minimum minigap opened in the normal metal DoS[35, 36], respectively. At large biases $|V| \gtrsim 0.5$ mV the resistance of the tunnel junction approaches the asymptotic normal-state value $R_T \approx 60$ kΩ. Figure 2(b) further shows an enlarged view of the flux dependence of the sub-gap current. Full phase modulation, i.e., complete suppression of the supercurrent at $\Phi = 0.5\,\Phi_0$, is observed due to the small Al loop inductance compared to that of the SNS weak link[11, 12]. The shape of the supercurrent peaks shows good agreement with a theoretical calculation (dotted lines) based on the $P(E)$ theory of incoherent Cooper pair tunneling[37, 38], assuming the junction to be embedded in an effective RC environment.

We next characterize the flux responsivity of the SQUIPT device by measuring current $I(\Phi)$ and voltage $V(\Phi)$ modulations at different values of bias voltage or current applied to the tunnel probe. Figure 2(c) and (e) illustrate some of such current and voltage modulations in the bias range from 0.246 mV to 0.369 mV and 0.14 nA to 7 nA, respectively. Furthermore, Fig. 2(d) shows the measured current modulation at several sub-gap bias voltages. With the $I(\Phi)$ and $V(\Phi)$ characteristics at hand, we obtain the flux-to-voltage transfer function $\partial V/\partial \Phi$ and flux-to-current transfer function $\partial I/\partial \Phi$ by numerical differentiation. The maximum absolute values $|\partial I/\partial \Phi|_{\text{max}} \simeq 8$ nA/Φ_0 and $|\partial V/\partial \Phi|_{\text{max}} \simeq 0.2$ mV/Φ_0 are reached at $V \approx 249\,\mu$V and $I \approx 4.2$ nA, respectively. The transfer functions close to these optimum bias values are plotted in Fig. 2(f) and (g), whereas the corresponding $I(\Phi)$ and $V(\Phi)$ characteristics are shown in bold in Fig. 2(c) and (e). Note that the maxima at $\Phi = n\,\Phi_0$ (with integer n) in the $V(\Phi)$ characteristics in panel (e) cross over to minima at higher bias currents, with analogous behavior evident in the current modulations in panel (b). This reflects the influence of the phase-dependent density of states on the IV characteristics at bias voltages slightly above the sum of the probe lead Al gap Δ and the proximity-induced minigap in the Cu wire.

Shot noise measurements. We now turn to a description of the SQUIPT noise measurements. For a tunnel junction-based device such as the SQUIPT, we expect the spectral density of the current shot noise to follow $S_{I_S} = 2e|I|$[22]. The blue dots in Fig. 3(a) show examples of measured spectral densities of voltage noise, referred to
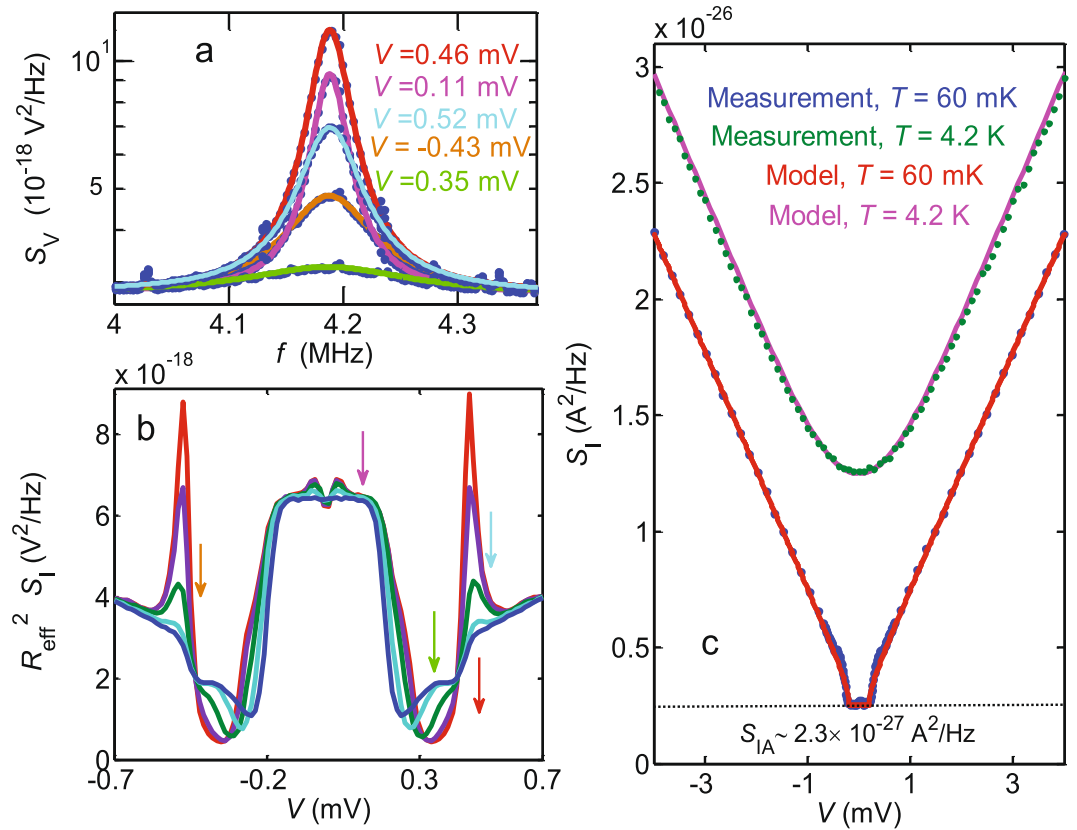
Figure 3. Noise measurements. (**a**) Power spectral density of the measured voltage noise at $\Phi = 0$ for the indicated values of the bias voltage V (blue dots), plotted on a semilogarithmic scale. The solid lines are fits to Eq. 1. (**b**) Bias dependence of the peak height $R_{eff}^2 S_I$, extracted from fits to Eq. 1, for a few equally spaced values of magnetic flux between $\Phi = 0$ (red solid line) and $\Phi = 0.5\,\Phi_0$ (blue solid line). (**c**) Total current noise S_I vs. the DC bias, measured at $T = 4.2\,K$ with the junction in the normal state, and at $T = 60\,mK$ in the superconducting state, together with the theoretical predictions (see text for details). The dashed horizontal line indicates the background noise level, independent of V and Φ.

the HEMT amplifier input. They were recorded at the base temperature with fixed magnetic flux $\Phi \approx 0$ through the interferometer loop, at the few indicated values of bias voltage V across the device. The solid lines result from nonlinear least squares fitting to[14]

$$S_V(f) = S_{V_A} + \frac{R_{eff}^2 S_I}{1 + (f^2 - f_0^2)^2 / (f\Delta f)^2},$$

(1)

showcasing how the white current noise S_I is filtered by the bandpass response of the RLC circuit, centered around f_0 (refer to Fig. 7 and subsequent discussion in the Methods Section for details). Above, S_{V_A} is the input voltage noise of the amplifier, $R_{eff} = (R_S^{-1} + R^{-1})^{-1}$ is the effective resistance in the circuit, and $S_I = S_{I_S} + S_{I_R} + S_{I_A}$ denotes the total current noise, composed of the current fluctuations of the sample (S_{I_S}), equilibrium noise of the parasitic resistance R ($S_{I_R} = 4k_B T/R$), and a background term (S_{I_A}), attributed to the amplifier current noise (see also Figs 8 and 9 and related discussion in the Methods Section). The current noise of the sample $S_{I_S} = S_{I_{shot}} + (\partial I/\partial \Phi)^2 S_\Phi$ can be further separated into shot noise $S_{I_{shot}}$ in the quasiparticle tunneling current, and external flux noise S_Φ mediated by the transfer function $\partial I/\partial \Phi$. Given the responsivity of the present sample, in our setup with f_0 in the MHz regime we expect the second term to be negligible. In the experiment, we have investigated the dependence of S_V and hence S_I on V, Φ, and T.

We make the fits to Eq. 1 using S_{V_A}, f_0, the peak height $P_0 = R_{eff}^2 S_I$, and the peak width $\Delta f = 2\pi L' f_0^2 / R_{eff}$ as adjustable parameters. Here, Δf gives directly the full width at half maximum (FWHM) of the peak in S_V in the limit $f_0 \gg \Delta f$. Of the four parameters, the background level $S_{V_A} \approx 3 \times 10^{-18}\,V^2/Hz$ due to the amplifier voltage noise, and the resonance frequency $f_0 \approx 4.18\,MHz$ can be kept fixed, whereas the peak height and width depend systematically on V, Φ, and T. With the fitting procedure established, Fig. 3(b) demonstrates typical bias dependence of the extracted values of the peak height P_0. The different curves correspond to a few equally spaced flux values between $\Phi = 0$ and $\Phi = 0.5\,\Phi_0$, whereas the vertical arrows indicate the bias voltages at $\Phi = 0$ for the spectra displayed in panel (a). It is noteworthy that the bias dependence of P_0 in Fig. 3(b) resembles that of $R_S(V, \Phi)$, i.e., the differential resistance of the sample. It arises due to the factor R_{eff}^2 in the definition of the peak height, and the fact that R_{eff} is a parallel combination of R_S and the constant parasitic resistance R.
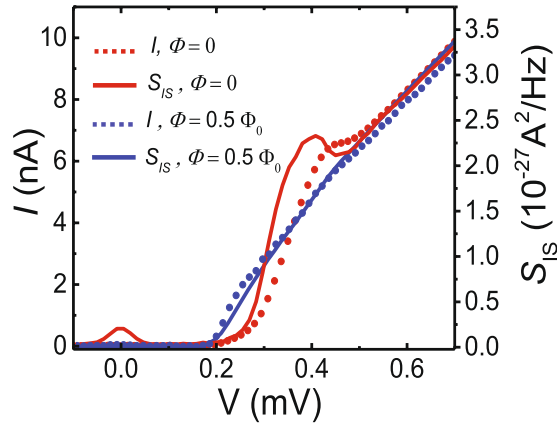
Figure 4. Bias dependence of the current noise. IV characteristics of the SQUIPT (red and blue dots) compared to the measured current noise S_{I_S} (red and blue solid lines) vs. bias voltage, at the two extreme flux values, $\Phi = 0$ and $\Phi = 0.5\,\Phi_0$.
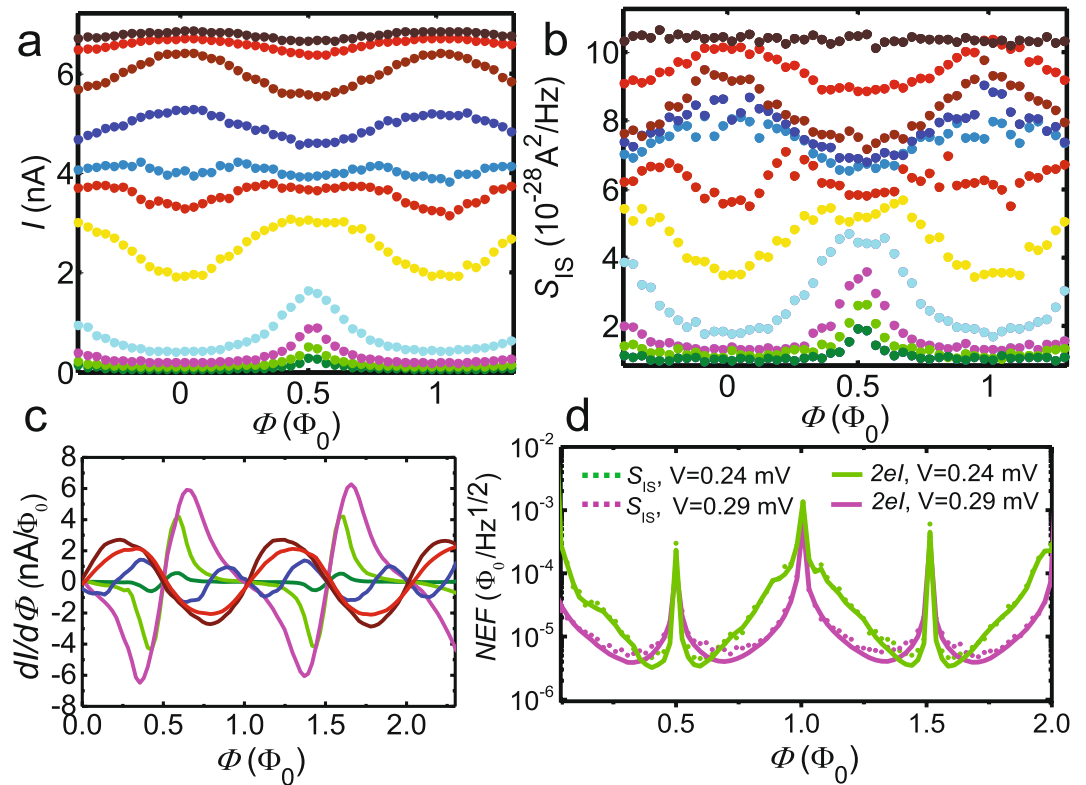

Figure 5. Characterization of flux noise performance of the voltage-biased SQUIPT device. **(a)** DC current and **(b)**, current noise as a function of magnetic flux at several values of bias voltage, measured simultaneously in the same setup at 60 mK. **(c)** Responsivity $\partial I/\partial \Phi$ at several biases. **(d)** Flux sensitivity at the 2nd and 3rd lowest bias voltages $V = 0.24$ mV and 0.29 mV in panels **(a–c)**. The dotted lines use S_{I_S} obtained by direct fitting of the measured S_V spectra, whereas the solid lines assume full shot noise $S_{I_S} = 2e|I(\Phi)|$ with $I(\Phi)$ from the DC measurement. Each color in panels (a)–(d) corresponds to a specific bias voltage.

Figure 3(c) shows the bias dependence of the total current noise S_I extracted in the above manner from noise spectra similar to those in panel (a). The two curves correspond to measurements at bath temperature $T = 4.2$ K with the SQUIPT fully in the normal state (top), and at the base temperature $T = 60$ mK (bottom) at a constant magnetic flux close to $\Phi = 0$. At $T = 4.2$ K, the measured noise is well explained by assuming $S_{I_S} = (2eV/R_T)coth(eV/2k_BT)$, shown by the pink solid line, see, e.g., ref. 22 and references therein. We use the high bias shot noise, i.e., the linear asymptotic increase of S_I with V, to calibrate the total gain of the setup, by requiring that the slope of S_I vs. V equals $2e|I|$. The value is in reasonable agreement with the nominal amplifier
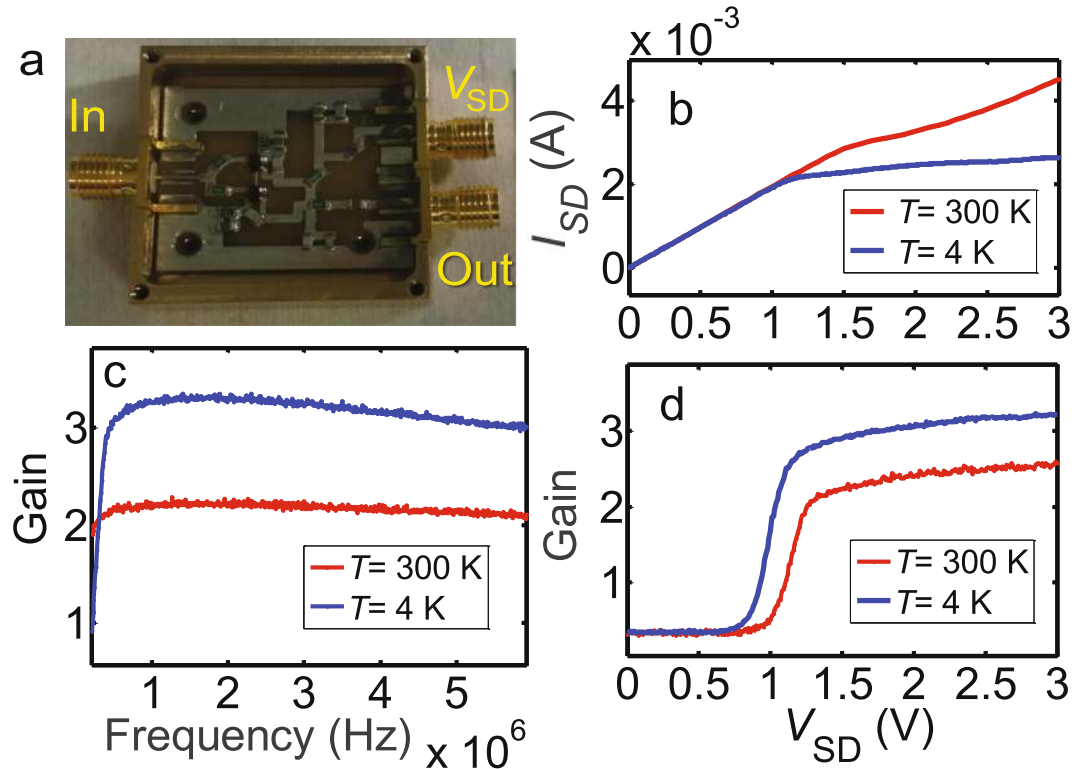
Figure 6. Cryogenic HEMT amplifier. **(a)** Inside view of the cryoamplifier with a pair of ATF-34143 HEMT transistors. **(b)** Source-drain current I_{SD} and **(d)** gain as a function of the supply voltage V_{SD} at two different temperatures $T = 4.2$ K (blue solid line) and $T = 300$ K (red solid line) at 3 MHz. By decreasing the temperature, I_{SD} decreases while the gain increases. **(c)** Frequency dependence of the gain at $V_{SD} = 2$ V at two different temperatures.

gains and expected losses in the circuit. At $T = 60$ mK we also find the noise to be dominated by the shot noise of the SQUIPT tunnel junction: Despite the nonlinear IV at $V \lesssim \Delta/e$, with increasing V the noise increases as $S_{I_S} \approx 2e|I(\Phi)|$. Here at $T = 60$ mK, for the theoretical model for simplicity we use the noise of an NIS tunnel junction, approximately valid for a SQUIPT at magnetic flux $\Phi = 0.5\,\Phi_0$ in which case the minigap in the normal metal vanishes[35, 36] (cf. subsection "Quasiparticle current fluctuations in a hybrid tunnel junction" under Methods). As evident in Fig. 3(c), at base temperature the expected $S_{I_R} \approx 0.7 \times 10^{-29}$ A²/Hz is much smaller than the background term $S_{I_A} \approx 2.3 \times 10^{-27}$ A²/Hz $\approx (48\,\text{fA})^2$/Hz. The origin of the large background current noise requires further study in future work: it is approximately an order of magnitude larger than the amplifier current noise $S_{I_A} \approx (13\,\text{fA})^2$/Hz found in Ref. Arakawa2013. It is notable that both the peak width Δf and height P_0 reflect strongly the bias- and flux-dependent changes in R_{eff} and hence $R_S(V, \Phi)$, cf. Figure 3(b). On the other hand, as illustrated by Fig. 3(c), the noise $S_I \propto P_0\Delta f^2$ calculated from these parameters follows $S_I \propto |I(\Phi)|$, highlighting the contribution of the shot noise of the tunnel junction.

In Fig. 4 we show the bias dependence of the noise in more detail at the two extreme flux values $\Phi = 0$ and $\Phi = 0.5\,\Phi_0$, noting that the shot noise directly reflects changes in the average current $I(V, \Phi)$. For an explicit comparison with the average current, we plot the corresponding IV characteristics in the same panel, showing that indeed $S_{I_S} \approx 2e|I|$. In particular this is well satisfied at $\Phi = 0.5\,\Phi_0$. In the S_{I_S} curve at $\Phi = 0$, we attribute the apparent excess noise around zero bias (at the gap edge) to an uncertainty in the fitting to extract the exact value of R_{eff} when the peak is at its narrowest (lowest height). It originates from the residual interfering peaks in the background noise of S_V, present for example at $f \approx 4.02$ MHz in Fig. 3(a).

Flux noise characterization. Two basic figures of merit of the SQUIPT are the transfer function $\partial I/\partial\Phi$ and the noise-equivalent flux $\text{NEF} = S_{I_S}^{1/2}/|\partial I/\partial\Phi|$ (flux sensitivity)[19]. To characterize the flux sensitivity of the device, we measure the flux dependence of $I(\Phi)$ and $S_{I_S}(\Phi)$ simultaneously in the same setup at several bias voltages V around the onset of the quasiparticle current. Examples of the resulting periodic modulations of I and S_{I_S} are shown in Fig. 5(a) and (b), respectively, demonstrating good qualitative agreement with $S_{I_S} \propto |I(\Phi)|$. Figure 5(c) further plots the flux-to-current transfer function $\partial I/\partial\Phi$, again obtained by numerical differentiation of $I(\Phi)$. With S_{I_S} and $\partial I/\partial\Phi$ at hand, we obtain the NEF curves shown in Fig. 5(d) for two bias values: $V = 0.24$ mV resulting in the lowest NEF (green), and $V = 0.29$ mV giving the highest $\partial I/\partial\Phi$. The dotted lines use S_{I_S} obtained by direct fitting of the measured S_V spectra as discussed above. On the other hand, considering the uncertainties in the fitting procedure, the solid lines assume full shot noise $S_{I_S} = 2e|I(\Phi)|$ with $I(\Phi)$ taken from the DC measurement.
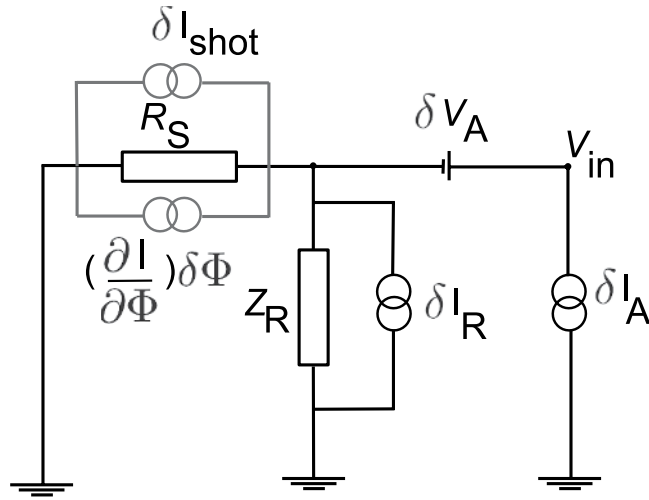
Figure 7. Circuit model for evaluating the voltage fluctuations referred to the amplifier input.
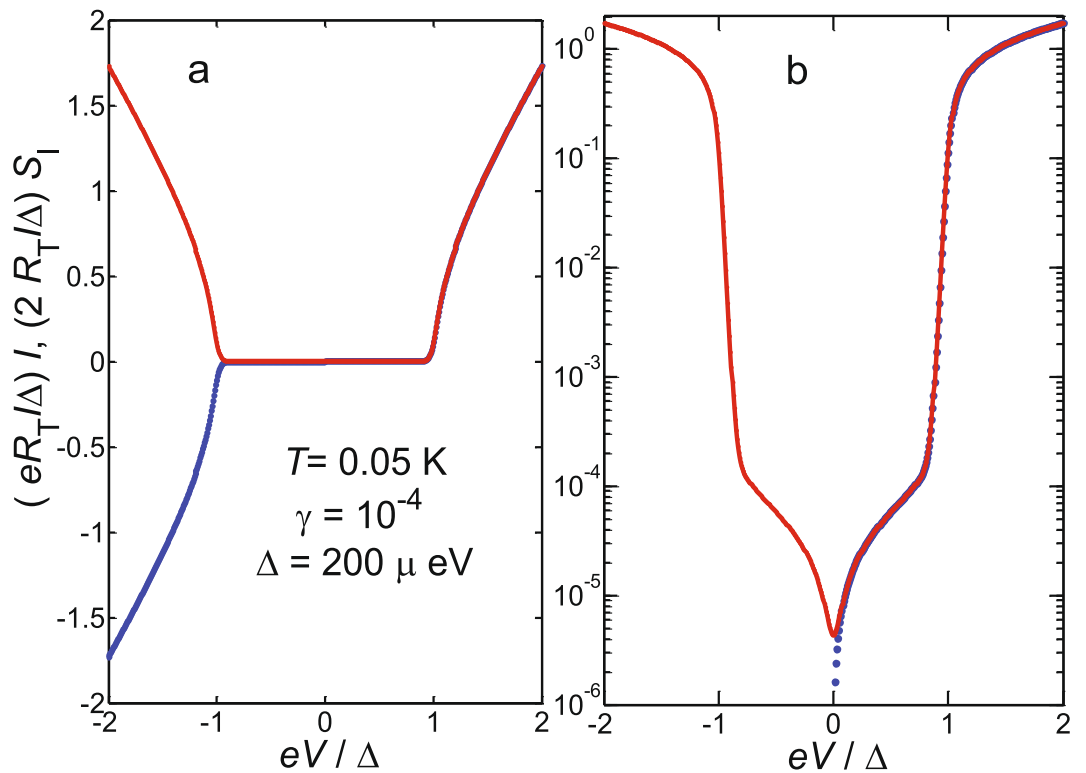

Figure 8. Current noise of a NIS junction. **(a)** Normalized IV characteristics of a NIS tunnel junction (blue dashed line) together with the current noise $S_{I_{shot}}$ (red solid lines) vs. bias voltage calculated at $T = 0.05$ K, with the superconducting Al gap $\Delta = 200\,\mu e$V. Here, the dimensionless parameter γ is the ratio between NIS junction asymptotic resistance at high bias voltage and the sub-gap resistance, used in the modeling of a smeared BCS density of states $n_S(E) = |\mathrm{Re}[(E/\Delta + i\gamma)/\sqrt{(E/\Delta + i\gamma)^2 - 1}]|$. **(b)** I and $S_{I_{shot}}$ as in (a) but plotted on a semilogarithmic scale.

A reasonable fit to the S_V spectra is obtained also under this assumption, resulting only in slight changes in the fitted values of R_{eff}.

We achieve the minimum value of NEF $\approx 4\,\mu\Phi_0/\text{Hz}^{1/2}$ (green solid/dotted line) at the optimum working point $V = 0.24$ mV, $\Phi \approx 0.4\,\Phi_0$. For comparison, low frequency ($f \sim 100$ Hz) flux noise NEF $\approx 0.5\,\mu\Phi_0/\text{Hz}^{1/2}$ has been reported for a current-biased, optimized Al-SQUIPT in a room-temperature cross correlation setup[12]. Likewise, improved flux sensitivity figures down to $\approx 50\,n\Phi_0/\text{Hz}^{1/2}$ have been recently reported for nanoSQUIDs[1–5]. Significant improvements to our initial demonstration of the MHz-range SQUIPT noise performance are
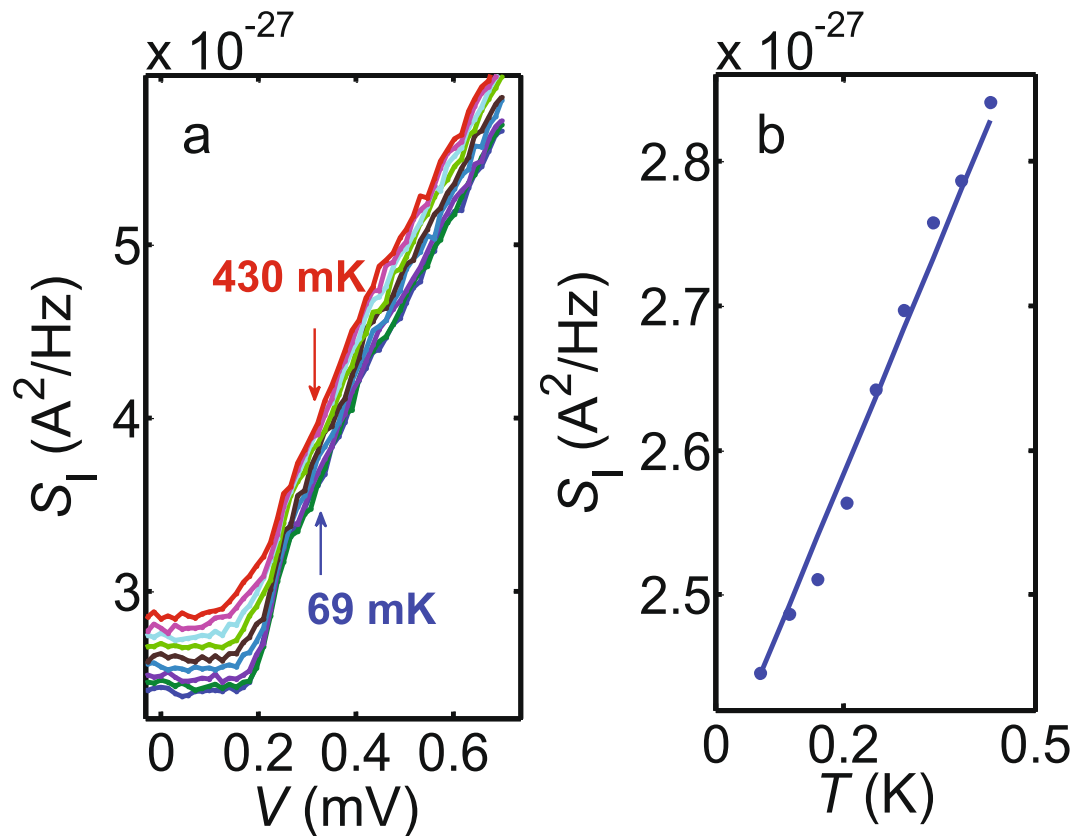
Figure 9. Temperature dependence of the total current noise. (**a**), Bias dependence of the total noise S_I at various values of the bath temperature at $\Phi \approx 0.5\,\Phi_0$. (**b**), Temperature dependence of S_I at $V = 0$ and $\Phi \approx 0.5\,\Phi_0$. As expected for thermal noise of R_{eff} ($\approx R$ at $V = 0$), the signal increases approximately linearly with slope $4k_B/R$ (solid blue line) with increasing T on top of a constant background $S_{I_A} \approx 2.3 \times 10^{-27}\,A^2/Hz$.

expected to result from optimizing the geometry of the device and the consequently enhanced responsivity[11–13]. For example, fabricating the interferometer loop from a larger-gap superconductor[39] and making a shorter normal metal wire[11, 12], the transfer function can be enhanced by a few orders up to $\mu A/\Phi_0$[12] under voltage bias, and flux noise in the $n\Phi_0/Hz^{1/2}$ range has been predicted[9, 13]. Similarly, for devices which reach the maximum responsivity in the supercurrent branch[39], we expect minimum values of the flux noise in the range of $50\,n\Phi_0/Hz^{1/2}$. Even higher-bandwidth readout of SQUIPT detectors, closely related to fast NIS tunnel junction thermometers[40–42], is possible by embedding the device in a lumped element or coplanar waveguide resonator with resonance frequency in the range of several hundred MHz or several GHz, respectively. This is similar to work on quantum-limited dispersive SQUID magnetometry with conventional Al tunnel junctions[43] or nanobridge weak links[44], with flux noise down close to $20\,n\Phi_0/Hz^{1/2}$ and bandwidth of the order of 10 MHz.

Discussion

In summary, we have investigated the flux noise performance of a SQUIPT interferometer based on shot noise measurements with a cryogenic amplifier at frequencies of the order of a few MHz. This represents the first noise study of such a hybrid interferometer not limited by the low-bandwidth room-temperature readout. The setup is capable of resolving the shot noise of a current $I \sim 100\,pA$ in a typical probe junction in an averaging time of the order of 30 s. In future work, the performance can be further improved by employing a lower-noise room-temperature amplifier, and by using the cross-correlation of signals from two low-temperature amplifiers to reject the uncorrelated background S_{V_A} while reliably picking out the signal due to S_{I_S}. In the present device we reach shot-noise-limited flux sensitivity of the order of $\mu\Phi_0/Hz^{1/2}$, which can be significantly improved upon optimizing the dimensions of the SNS weak link and the readout tunnel probe.

Methods

Fabrication details. The sample is fabricated using electron beam lithography (EBL) and electron beam evaporation of the Al and Cu thin films. A single lithography step relying on a Ge based hard mask is used to define patterns for multi-angle shadow evaporation of the NIS tunnel probe and the proximity SNS weak link in a single vacuum cycle. The starting point is an oxidized Si substrate onto which we first spin coat a 900 nm thick layer of P(MMA-MAA) copolymer. Subsequently, a 22 nm thick film of Ge is deposited by electron beam evaporation, followed by spin coating a 50 nm thick polymethyl methacrylate (PMMA) layer. The EBL step is followed by first developing the chip in 1:3 solution of methyl isobutyl ketone (MIBK) and isopropanol (IPA) for 30 s,

rinsing in IPA and drying. Reactive ion etching (RIE) with CF_4 (for Ge) and O_2 (for the copolymer layer) is then used to create a suspended mask with proper undercut profile for shadow evaporation. The metals are deposited by electron-beam evaporation: first, 25 nm of Al is deposited and oxidized *in-situ* for 1 min with pure oxygen pressure of 1 millibar to form the tunnel barrier of the normal metal-insulator-superconductor (NIS) probe. Next, approximately 15 nm of copper is evaporated to complete the NIS junction and to form the normal metal part of the SNS proximity weak link. Immediately after this, the superconducting Al loop with 120 nm thickness is deposited to form clean contacts to the copper island, which completes the structure. Figure 1(a) shows an SEM image of a resulting SQUIPT device, illustrating the thick Al loop interrupted by the short Cu wire, as well as the thin Al tunnel probe electrode in the middle.

Cryogenic HEMT amplifier.

The design of our cryogenic amplifier follows directly the one introduced in Ref. Arakawa2013. The device consists of passive components including surface mount metal-film resistors and laminated ceramic capacitors, and two Avago ATF-34143 high-electron-mobility transistors as the only active elements. The PCB board is placed in a brass shield box with the outer size 34 mm × 34 mm [see Fig. 6(a)]. In order to reduce 1/f noise of the amplifier, we prepared the double-HEMT amplifier using two transistors in parallel[17].

The typical source-drain current I_{SD} [Fig. 6(b)] and gain [Fig. 6(d)] as a function of the supply voltage V_{SD} are plotted at two different temperatures $T = 4.2$ K (blue solid lines) and $T = 300$ K (red solid lines) at 3 MHz. As observed in Ref. Arakawa2013, at low temperatures I_{SD} reduces while the gain increases. Furthermore, the gain varies only weakly in the saturation region $V_{SD} \gtrsim 1.2$ V. For the noise measurement setup, we prepared the LC resonance circuit with the resonant frequency to be close to 4 MHz. Figure 6(c) shows the frequency dependence of the gain at $V_{SD} = 2$ V, remaining approximately constant (~3.4 at $T = 4.2$ K) at the frequencies of interest.

Model for evaluating the spectrum of voltage noise.

Figure 7 shows a simplified circuit model of the setup in Fig. 1(b), including relevant noise sources for calculating the total voltage noise probed by the HEMT amplifier at its input. Here, it is assumed that the capacitors C_c and C_l behave as shorts at frequencies close to f_0, whereas Z_R denotes the impedance of the parallel RLC circuit, defined via

$$1/Z_R(\omega) = 1/R + 1/(i\omega L') + i\omega C_{coax}, \tag{2}$$

with $\omega = 2\pi f$. The cryogenic amplifier probes the voltage V_{in}, applied to the gate of its HEMT transistor. The amplifier input voltage and current noise spectral densities are denoted by S_{V_A} and S_{I_A}, respectively. In the following they will be assumed to be white at the frequencies of interest $f \sim f_0$. δV_A and δI_A represent the corresponding voltage and current noise sources. In Fig. 7, the input impedance of the amplifier is assumed to be high. The equilibrium current fluctuations in the RLC circuit (i.e., the resistance R) are denoted by δI_R, with spectral density S_{I_R}. For the total sample noise we write $\delta I_S = \delta I_{shot} + (\partial I/\partial\Phi)\delta\Phi$, corresponding to $S_{I_S} = S_{I_{shot}} + (\partial I/\partial\Phi)^2 S_\Phi$.

It is now straightforward to write down Kirchhoff's laws for the circuit. Considering the voltage fluctuation $\Delta V_{in}(\omega)$ at the amplifier input, we have

$$\Delta V_{in}(\omega) = Z_{eff}(\omega)[\delta I_S + \delta I_R + \delta I_A] + \delta V_A. \tag{3}$$

Here $Z_{eff}(\omega)$ is the parallel impedance of the sample and the RLC circuit

$$1/Z_{eff}(\omega) = 1/R_S + 1/Z_R(\omega). \tag{4}$$

Equation 3 now directly yields the spectral density of the total voltage fluctuations at the amplifier input as

$$S_V(\omega) = Z_{eff}(\omega)Z_{eff}(-\omega)\left[S_{I_S} + S_{I_R} + S_{I_A}\right] + S_{V_A}. \tag{5}$$

Noting the definition of the effective resistance $R_{eff} = (R_S^{-1} + R^{-1})^{-1}$ and Eq. 2, we see that Eq. 5 can be explicitly rewritten to obtain Eq. 1 in the main text.

Quasiparticle current fluctuations in a hybrid tunnel junction.

Here we show that despite the non-constant densities of states in both electrodes of the SQUIPT tunnel junction and the nonlinear IV characteristic, the simple approximation $S_{I_{shot}} \approx 2e|I|$ still holds down to relatively low sub-gap bias voltages V. In the SNS proximity junction, the density of states $n_N(\varepsilon, \phi)$ in the proximized normal metal depends on the phase difference ϕ between the S electrodes. This phase- and hence flux-dependent DoS is probed by a tunnel junction with a pure superconducting counterelectrode with the BCS DoS $n_S(\varepsilon)$, biased by voltage V. Starting from a generic tunnel Hamiltonian, the current noise for a SQUIPT with tunnel resistance R_T can be written as

$$S_{I_{shot}}(\omega, V, \phi) = 2R_T^{-1}\int d\varepsilon\, n_N(\varepsilon, \phi)n_S(\varepsilon - eV)\{f(\varepsilon - eV)[1 - f(\varepsilon + \hbar\omega)]$$
$$+ [1 - f(\varepsilon - eV)]f(\varepsilon - \hbar\omega)\}. \tag{6}$$

Here we assume a narrow probe electrode and neglect the dependence of $n_N(\varepsilon, \phi)$ on the position along the SNS junction[10, 13]. In Eq. 6, $f(\varepsilon) = 1/[\exp(\varepsilon/k_B T_e) + 1]$ denotes the Fermi-Dirac (quasi-) equilibrium distribution function where T_e and k_B are electron temperature and Boltzmann constant, respectively. We further assume the low frequency limit $\hbar\omega \ll k_B T_e, eV, \Delta$, yielding

$$S_{I_{shot}}(V, \phi) = 2R_T^{-1} \int d\varepsilon\, n_N(\varepsilon, \phi)\, n_S(\varepsilon - eV)\{f(\varepsilon - eV)[1 - f(\varepsilon)] + [1 - f(\varepsilon - eV)]f(\varepsilon)\}. \tag{7}$$

For simplicity, let us consider the SQUIPT device at magnetic flux $\Phi = 0.5\,\Phi_0$, in which case we approximate $n_N = 1$ and obtain

$$S_{I_{shot}}(V) = 2R_T^{-1} \int d\varepsilon\, n_S(\varepsilon)\{f(\varepsilon - eV)[1 - f(\varepsilon)] + [1 - f(\varepsilon - eV)]f(\varepsilon)\}. \tag{8}$$

Figure 8 displays the IV characteristics of such a NIS tunnel junction together with the current noise from Eq. 8 calculated at $T_e = 0.05\,K$, assuming the superconducting Al gap $\Delta = 200\,\mu eV$. For an NIN junction we can further set $n_N = n_S = 1$, resulting in

$$S_{I_{shot}}(V) = 2R_T^{-1} \int d\varepsilon\{f(\varepsilon - eV)[1 - f(\varepsilon)] + [1 - f(\varepsilon - eV)]f(\varepsilon)\}. \tag{9}$$

This can be directly integrated to yield $S_{I_{shot}} = (2eV/R_T)coth(eV/2k_BT_e)$. Two basic cases are then immediately obtained from this expression, namely (i) for $e|V| \ll k_BT_e$ the equilibrium thermal noise $4k_BT_e/R_T$, and (ii) full shot noise $2e|I|$ in the limit $e|V| \gg k_BT_e$.

Temperature dependence of the total current noise. Besides the measurements at $T = 4.2\,K$ and $T = 60\,mK$ discussed in the main text, we have probed the total current noise $S_I = S_{I_S} + S_{I_R} + S_{I_A}$ at $\Phi \approx 0.5\,\Phi_0$ in a range of bath temperatures below 500 mK. Figure 9(a) plots the bias dependence of S_I for various bath temperatures T between 69 mK and 430 mK. At each bias we observe a slight increase in S_I towards higher T, whereas the V-dependence is always dominated by the shot noise of the SQUIPT probe junction. The background term S_{I_A} is expected to be independent of the sample holder temperature, and S_{I_S} has only weak temperature dependence at bias voltages around the gap edge. Hence, most of the T-dependence in Fig. 9(a) should be determined by $S_{I_R} = 4k_BT/R$. This is supported by Fig. 9(b) where we plot the values of S_I at $V = 0$. At zero bias, the sample noise $S_{I_S} = 4k_BT/R_S$ is negligible compared to S_{I_R} due to $R_S \gg R$ at sub-gap voltages. The measured temperature dependence of the zero-bias noise agrees with $S_I = S_{I_R} + S_{I_A}$, i.e., a linear increase with slope $4k_B/R$, on top of a background set by S_{I_A}.

References

1. Martínez-Pérez, M. J. & Koelle, D. NanoSQUIDs: Basics & recent advances, arXiv:1609.06182 (2016).
2. Schmelz, M. *et al.* Investigation of all niobium nano-SQUIDs based on sub-micrometer cross-type Josephson junctions. *Supercond. Sci. Technol.* **28**, 015004 (2015).
3. Martínez-Pérez, M. J. *et al.* NanoSQUID magnetometry of individual cobalt nanoparticles grown by focused electron beam induced deposition. *Supercond. Sci. Technol.* **30**, 024003 (2017).
4. Schmelz, M. *et al.* Nearly quantum limited nanoSQUIDs based on cross-type Nb/AlOx/Nb junctions. *Supercond. Sci. Technol.* **30**, 014001 (2017).
5. Vasyukov, D. *et al.* A scanning superconducting quantum interference device with single electron spin sensitivity. *Nat. Nanotech.* **8**, 639 (2013).
6. Petrashov, V. T., Antonov, V. N., Delsing, P. & Claeson, T. Phase controlled mesoscopic ring interferometer. *JETP Lett.* **59**, 551 (1994).
7. Petrashov, V. T., Antonov, V. N., Delsing, P. & Claeson, T. Phase Controlled Conductance of Mesoscopic Structures with Superconducting Mirrors. *Phys. Rev. Lett.* **74**, 5268 (1995).
8. Tinkham, M. Introduction to Superconductivity, 2nd Ed. (McGraw-Hill, New York, 1996).
9. Giazotto, F., Peltonen, J. T., Meschke, M. & Pekola, J. P. Superconducting quantum interference proximity transistor. *Nat. Phys.* **6**, 254 (2010).
10. Meschke, M., Peltonen, J. T., Pekola, J. P. & Giazotto, F. Tunnel spectroscopy of a proximity Josephson junction. *Phys. Rev. B* **84**, 214514 (2011).
11. Jabdaraghi, R. N., Meschke, M. & Pekola, J. P. Non-hysteretic superconducting quantum interference proximity transistor with enhanced responsivity. *Appl. Phys. Lett.* **104**, 082601 (2014).
12. Ronzani, A., Altimiras, C. & Giazotto, F. Highly-sensitive superconducting quantum interference proximity transistor. *Phys. Rev. Appl.* **2**, 024005 (2014).
13. Giazotto, F. & Taddei, F. Hybrid superconducting quantum magnetometer. *Phys. Rev. B* **84**, 214502 (2011).
14. DiCarlo, L. *et al.* System for measuring auto- and cross correlation of current noise at low temperatures. *Rev. Sci. Instrum.* **77**, 073906 (2006).
15. Hashisaka, M. *et al.* Development of a measurement system for quantum shot noise at low temperatures. *Phys. Stat. Sol. (c).* **5**, 128 (2008).
16. Hashisaka, M. *et al.* Measurement for quantum shot noise in a quantum point contact at low temperatures. *J. Phys.: Conf. Ser.* **109**, 012013 (2008).
17. Arakawa, T., Nishihara, Y., Maeda, M., Norimoto, S. & Kobayashi, K. Cryogenic amplifier for shot noise measurement at 20 mK. *Appl. Phys. Lett.* **103**, 172104 (2013).
18. Belzig, W., Wilhelm, F. K., Bruder, C., Schön, G. & Zaikin, A. D. Corrigendum to Quasiclassical Green's function approach to mesoscopic superconductivity. *Superlatt. Microstruct.* **25**, 1251 (1999).
19. Likharev, K. K. Dynamics of Josephson Junctions and Circuits (Gordon and Breach, 1986).
20. Ronzani, A., Altimiras, C., D'Ambrosio, S., Virtanen, P. & Giazotto, F. Phase-driven collapse of the Cooper condensate in a nanosized superconductor. arXiv:1611.06263 (2016).
21. Schottky, W. Regarding spontaneous current fluctuation in different electricity conductors. *Ann. Phys.* **57**, 541 (1918).
22. Blanter, Y. M. & Büttiker, M. Shot noise in mesoscopic conductors. *Phys. Rep.* **336**, 15 (2000).
23. Landauer, R. Condensed-matter physics: The noise is the signal. *Nature* **392**, 658 (1998).
24. Reznikov, M., Heiblum, M., Shtrikman, H. & Mahalu, D. Temporal Correlation of Electrons: Suppression of Shot Noise in a Ballistic Quantum Point Contact. *Phys. Rev. Lett.* **75**, 3340 (1995).
25. Kumar, A., Saminadayar, L. & Glattli, D. C. Experimental test of the quantum shot noise reduction theory. *Phys. Rev. Lett.* **76**, 15 (1996).

26. Zarchin, O., Zaffalon, M., Heiblum, M., Mahalu, D. & Umansky, V. Two-electron bunching in transport through a quantum dot induced by Kondo correlations. *Phys. Rev. B* **77**, 241303(R) (2008).
27. Spietz, L., Lehnert, K. W., Siddiqi, I. & Schoelkopf, R. J. Primary electron thermometry using the shot noise of a tunnel junction. *Science* **300**, 1929 (2003).
28. Spietz, L., Schoelkopf, R. J. & Pari, P. Shot noise thermometry down to 10 mK. *Appl. Phys. Lett.* **89**, 183123 (2006).
29. Iftikhar, Z. *et al.* Primary thermometry triad at 6 mK in mesoscopic circuits. *Nat. Commun.* **7**, 12908 (2016).
30. Nishihara, Y. *et al.* Shot noise suppression in InGaAs/InGaAsP quantum channels. *Appl. Phys. Lett.* **100**, 203111 (2012).
31. Nakamura, S. *et al.* Conductance anomaly and Fano factor reduction in quantum point contacts. *Phys. Rev. B* **79**, 201308(R) (2009).
32. Yamauchi, Y. *et al.* Evolution of the Kondo Effect in a Quantum Dot Probed by Shot Noise. *Phys. Rev. Lett.* **106**, 176601 (2011).
33. Okazaki, Y., Sasaki, S. & Muraki, K. Shot noise spectroscopy on a semiconductor quantum dot in the elastic and inelastic cotunneling regimes. *Phys. Rev. B* **87**, 041302(R) (2013).
34. Jezouin, S. *et al.* Quantum Limit of Heat Flow Across a Single Electronic Channel. *Science* **342**, 601 (2013).
35. le Sueur, H., Joyez, P., Pothier, H., Urbina, C. & Esteve, D. Phase Controlled Superconducting Proximity Effect Probed by Tunneling Spectroscopy. *Phys. Rev. Lett.* **100**, 197002 (2008).
36. Zhou, F., Charlat, P., Spivak, B. & Pannetier, B. Density of States in Superconductor-Normal Metal-Superconductor Junctions. *J. Low Temp. Phys.* **110**, 841 (1998).
37. Averin, D. V., Nazarov, Y. V. & Odintsov, A. A. Incoherent tunneling of the Cooper pairs and magnetic flux quanta in ultrasmall Josephson junctions. *Physica (Amsterdam)* **165B166B**, 945 (1990).
38. Ingold, G. L. & Nazarov, Y. V. In Single Charge Tunneling, NATO ASI Series B, Vol. **294**, edited by Grabert, H. & Devoret, M. H., pp. 21–107 (Plenum, New York, 1992).
39. Jabdaraghi, R. N., Peltonen, J. T., Saira, O.-P. & Pekola, J. P. Low-temperature characterization of Nb-Cu-Nb weak links with Ar ion-cleaned interfaces. *Appl. Phys. Lett.* **108**, 042604 (2016).
40. Schmidt, D. R., Yung, C. S. & Cleland, A. N. Nanoscale radio-frequency thermometry. *Appl. Phys. Lett.* **83**, 1002 (2003).
41. Gasparinetti, S. *et al.* Fast Electron Thermometry for Ultrasensitive Calorimetric Detection. *Phys. Rev. Appl.* **3**, 014007 (2015).
42. Saira, O.-P., Zgirski, M., Viisanen, K. L., Golubev, D. S. & Pekola, J. P. Dispersive Thermometry with a Josephson Junction Coupled to a Resonator. *Phys. Rev. Appl.* **6**, 024005 (2016).
43. Hatridge, M., Vijay, R., Slichter, D. H., Clarke, J. & Siddiqi, I. Dispersive magnetometry with a quantum limited SQUID parametric amplifier. *Phys. Rev. B.* **83**, 134501 (2011).
44. Levenson-Falk, E. M., Antler, N. & Siddiqi, I. Dispersive nanoSQUID magnetometry. *Supercond. Sci. Technol.* **29**, 113003 (2016).

Acknowledgements

Author Contributions

R.N.J. fabricated the device. R.N.J. and J.T.P. performed the experiments, analyzed the data, and wrote the manuscript. D.S.G. and J.P.P. provided theory support. J.P.P. discussed at all stages of the measurement with R.N.J. and J.T.P. All authors discussed the results and their implications, and contributed to editing the manuscript.

Additional Information

Competing Interests: The authors declare that they have no competing interests.

Publisher's note: Springer Nature remains neutral with regard to jurisdictional claims in published maps and institutional affiliations.